Forensic Science International 327 (2021) 110984

Contents lists available at ScienceDirect

Forensic Science International

journal homepage: www.elsevier.com/locate/forsciint

3Tesla post-mortem MRI quantification of anatomical brain structures

Isabel Arnold[a], Nicole Schwendener[a], Paolo Lombardo[a,b], Christian Jackowski[a], Wolf-Dieter Zech[a,*]

[a] Institute of Forensic Medicine, University of Bern, Switzerland
[b] Department of Diagnostic, Interventional and Pediatric Radiology, University of Bern, Inselspital Bern, Switzerland

ARTICLE INFO

Article history:
Received 27 October 2020
Received in revised form 4 March 2021
Accepted 17 August 2021
Available online 27 August 2021

Keywords:
Brain
Post-mortem magnetic resonance quantification
Post-mortem magnetic resonance neuroimaging

ABSTRACT

Quantitative post-mortem magnetic resonance imaging (PMMR) allows for measurement of T1 and T2 relaxation times and proton density (PD) of brain tissue. Quantitative PMMR values may be used for advanced post-mortem neuro-imaging diagnostics such as computer aided diagnosis. So far, the quantitative T1, T2 and PD post-mortem values of regular anatomical brain structures were unknown for a 3 Tesla PMMR application. The goal of this basic research study was to evaluate the quantitative values of post-mortem brain structures for a 3 T post-mortem magnetic resonance application with regard to various corpse temperatures. In 50 forensic cases, a quantitative PMMR brain sequence was applied prior to autopsy. Measurements of T1 (in ms), T2 (in ms), and PD (in %) values of cerebrum (Group 1: frontal grey matter, frontal white matter, thalamus, caudate nucleus, globus pallidus, putamen, internal capsule) brainstem and cerebellum (Group 2: cerebral peduncle, substantia nigra, red nucleus, pons, middle cerebellar peduncle, cerebellar hemisphere, medulla oblongata) were conducted in synthetically calculated axial PMMR brain images. Assessed quantitative values were corrected for corpse temperature. Temperature dependence was observed mainly for T1 values. ANOVA testing resulted in significant differences of quantitative values between the investigated anatomical brain structures in both groups. It can be concluded that temperature corrected 3 Tesla PMMR T1, T2 and PD values are feasible for characterization and discrimination of regular anatomical brain structures. This may provide a base for future advanced diagnostics of forensically relevant brain lesions and pathology.

1. Introduction

In the last two decades, post-mortem magnetic resonance imaging (PMMR) has been recognized as a potential useful adjunct to autopsy, particularly in natural causes of death [1–7]. Currently, post-mortem computed tomography and PMMR cannot generally replace traditional autopsy but may provide an alternative to autopsy in specific cases [8–13]. In the forensic field, PMMR research mainly focused on brain and heart since both organs frequently exhibit forensic relevant findings [2,7,14–20]. In recent years, quantitative MR-sequences were introduced to PMMR. Specific quantitative sequences allow for simultaneous assessment of vendor independent T1 and T2 relaxation times (in milliseconds) and Proton density (PD in %, where 100% is equivalent to pure water) of tissues within synthetically calculated MR images [21–25]. With dedicated software, measurements of quantitative values can be conducted in synthetically calculated MR images. Quantitative T1, T2 and PD values are dependent on tissue property such as water content. Thus, specific tissues and organs exhibit specific T1, T2 and PD values. In pathologic lesions, changes of tissue property may result in alteration of quantitative T1, T2 and PD values as compared to regular tissue. For instance, recent quantitative PMMR studies of the heart showed that quantitative T1, T2 and PD values of regular myocardium significantly differed to values of different histopathological stages of myocardial infarction such as ischemia, necrosis, scar tissue and hemorrhage. Acute myocardial infarction with edema and hemorrhage resulted in a significant increase of T1, T2 and PD values compared to regular myocardium [26–29]. Based on these studies, it can be hypothesized that brain pathology may as well be assessed and characterized by their quantitative T1, T2 and PD values. So far, quantitative PMMR values of brain pathology and trauma have not been investigated yet. However, assessment of brain pathology is only useful if it is comparable to quantitative values of regular brain tissue. Thus, there is a need assessing not only brain pathology values but also regular brain values. Due to the anatomic conditions of

* Correspondence to: University of Bern, Institute of Forensic Medicine Bern, Murtentenstrasse 26, 3008 Bern, Switzerland.
E-mail address: Wolf-Dieter.Zech@irm.unibe.ch (W.-D. Zech).

https://doi.org/10.1016/j.forsciint.2021.110984
0379-0738/

the brain with its various specific neuroanatomical structures that may all exhibit specific quantitative values, assessment of regular brain structures is rather complex. Therefore, it seems suitable to investigate regular quantitative brain values separately. A recent 1.5 Tesla PMMR study assessed regular anatomical brain structures of cerebrum, brainstem and cerebellum. The study showed that the numerous regular brain structures exhibited specific T1, T2 and PD values. Moreover, the investigated structures were discernable among each other based on a combination of their quantitative values [30]. While 1.5 T post-mortem brain values are known, post-mortem 3 T regular brain values remained unknown so far. Currently, both 1.5 Tesla and 3 Tesla MR machines are being used in post-mortem imaging [1,9,28,29]. Since T1 and T2 relaxation times are dependent on magnetic field strength [31], T1 and T2 relaxation times of the same tissue differ between 1.5 T and 3 T PMMR applications [29,30]. As a means to use quantitative PMMR in post-mortem imaging practice, quantitative T1, T2 and PD values of regular anatomical brain structures as well as brain pathologies need to be known for both 1.5 T and 3 T applications. Thus, there is a need assessing the regular quantitative post-mortem values for 3 Tesla applications which is the subject of this study. Quantitative values, especially T1 values, have shown to be temperature dependent for various tissues including the brain. In forensic practice, scanned corpses usually exhibit different body temperatures. In order to compare corpses with different body temperatures, there is a need for temperature correction of quantitative values [26,32–34]. Thus, the goal of this basic research study was to evaluate the quantitative values of post-mortem regular brain structures for a 3 T post-mortem magnetic resonance application with regard to various corpse temperatures.

2. Methods and materials

2.1. Study subjects

In this prospective study, the study subjects consisted of 50 forensic cases (31 males, 19 females; age 20–68 years, mean age 52.3 years) from the authors forensic host institution. Study subject inclusion criteria were as follows: brains appearing unremarkable at PMMR (no intracranial free gas accumulations or gas in head and brain vessels) and autopsy; no brain injuries or brain pathologies. Causes of death were cardiac arrest (n = 34), myocardial infarction (n = 5), thoracic trauma (n = 6) and abdominal trauma (n = 5). The time between death and post-mortem magnetic resonance imaging ranged from 1 to 4 days.

2.2. Post-mortem MRI and temperature measurements

The MR-Scanner used was a 3 Tesla Ingenia (Philips Healthcare, Best, the Netherlands) using 16-channel head / base combination. Corpses were examined in supine position. The quantification sequence used was a multi-echo, multi-slice turbo spin echo (TSE) sequence, with a saturation pre-pulse. Each acquisition was performed with two different echo times at 13 and 100 ms. Four different saturation delay times were acquired at 210, 610, 1820, and 3830 ms, using a TR of 4876 ms, resulting in a matrix with various effects of T1 and T2 relaxation. The FOV was 230 × 187 mm, acquired at a resolution of 0.7 × 0.9 mm and reconstructed at a resolution of 0.53 mm. 30 slices were acquired. Slice thickness was 4.5 mm (gap 0.5 mm). Scan time of the quantification sequence was 7 min. The raw images were post-processed using the commercially available SyMRI® 8.0 (Synthetic MR, Linköping/ Sweden) tool to retrieve T1 and T2 relaxation maps, as well as PD maps. The effects of B1 inhomogeneity, coil sensitivity profile, spurious echoes, and imperfect pulse profile effects were automatically corrected for. Based on the maps, synthetic T1-weighted, T2-weighted, and PD-weighted images were generated. During PMMR, corpse core temperatures were measured with a MR proof temperature probe (Temperature Transmitter FTX-300, Fiber Optic Temperature Probe PRB-MR1, Osensa Innovations, Canada) placed into the esophagus.

2.3. Autopsy and histology

Board certified forensic pathologists conducted autopsies subsequent to PMMR. At autopsy, Flechsig technique was used to remove the brain from the scull cavity. Dissection of both brain halves was conducted by parallel slicing. Brain tissue samples from frontal cortex, hippocampus, cerebellum, and pons were taken for histologic examinations (stain Hematoxylin and Eosin (H&E)). Board certified forensic pathologists blinded to PMMR results evaluated brain histology.

2.4. Quantitative value measurements

Measurements of T1 (in ms), T2 (in ms), and PD (in %) values of anatomical brain structures were conducted in synthetically calculated axial brain images by one observer. According to Zech et al. [30], anatomical brain structures were categorized into two groups. Group 1 included cerebral structures (frontal grey matter, frontal white matter, thalamus, caudate nucleus, globus pallidus, putamen and internal capsule). Group 2 included cerebellar structures and brain stem structures (cerebral peduncle, substantia nigra, red nucleus, pons, middle cerebellar peduncle, cerebellar hemisphere, and medulla oblongata). Six regions of interest (ROIs, size depending on expansion of brain structure, minimum size: 3 millimeters, maximum size: 10 millimeters) were placed in each anatomical structure in three adjacent slices (Fig. 1). One observer (forensic pathologist resident with two years of experience in post-mortem imaging) conducted measurements on all cases. A second observer (observer two (forensic pathologist with 10 years of experience in PMMR)) conducted additional measurements on 20 random cases of the study group for inter-observer analysis.

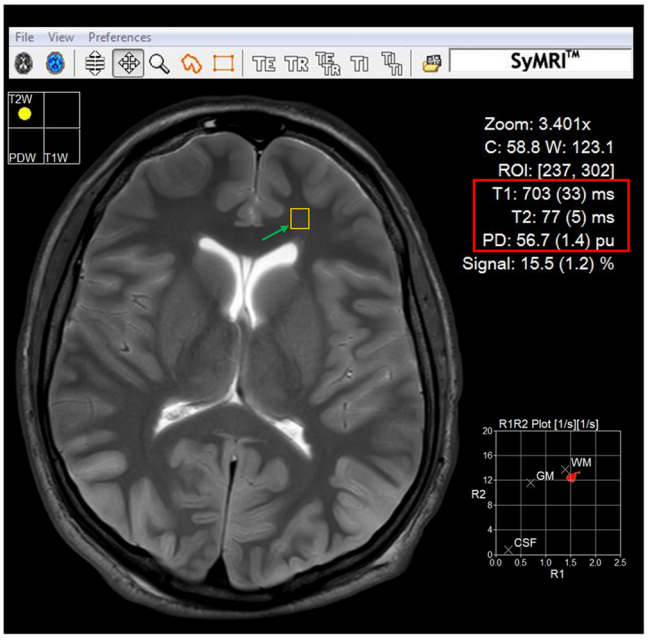

Fig. 1. Exemplary quantitative measurement of white matter in a synthetically calculated T2w PMMR image. Quantitative values were obtained by placing a square ROI (green arrow) into the dedicated anatomic region. T1 and T2 values (both in ms) and PD (as %) of the measured region are given by the software in the upper right corner (red frame) of the image. (For interpretation of the references to colour in this figure legend, the reader is referred to the web version of this article.)

Table 1
Equations generated from the relation of T1, T2, and PD plots to body core temperature (y: value corrected to 37 °C; T1: T1 relaxation time in milliseconds, T2: T2 relaxation time in milliseconds, T: body core temperature in °C, PD: proton density in % related to pure water (100%).

	T1 / temperature	T2 / temperature	PD / temperature
Group 1			
Grey matter	y = 9.8 T + 885	y = 0.3 T + 118	y = 0.8 T + 60
White matter	y = 3.2 T + 655	y = 0.2 T + 83	y = 0.3 T + 50
Thalamus	y = 4.4 T + 644	y = 0.4 T + 70	y = 0.2 T + 61
Caudate nucleus	y = 6.1 T + 717	y = 0.5 + 76	y = 0.2 T + 64
Globus pallidus	y = 6.9 T + 554	y = 0.3 T + 58	y = 0.4 T + 52
Putamen	y = 5.5 T + 562	y = 0.1 T + 55	y = 0.4 T + 62
Internal capsule	y = 3.8 T + 699	y = 0.3 T + 85	y = 0.3 T + 48
Group 2			
Cerebral peduncle	y = 7.3 T + 819	y = 0.4 T + 106	y = 0.3 T + 62
Substantia nigra	y = 7.7 T + 656	y = 0.1 T + 86	y = 0.4 T + 48
Red nucleus	y = 6.2 T + 657	y = 0.5 T + 93	y = 0.3 T + 45
Pons	y = 5.2 T + 700	y = 0.6 T + 88	y = 0.2 T + 54
Middle cerebellar peduncle	y = 4.8 T + 702	y = 0.1 T + 90	y = 0.3 T + 54
Cerebellum	y = 7.9 T + 676	y = 0.1 T + 69	y = 0.3 T + 62
Medulla	y = 6.2 T + 784	y = 0.6 T + 95	y = 0.2 T + 67

2.5. Corpse temperatures and temperature correction

Measured core temperatures of 50 corpses ranged between 7 °C and 33 °C with a mean temperature of 17 °C at the time of PMMR. PMMR examination did not result in corpse core temperature increases larger than one degree Celsius. Mean temperature values of seven measurements (one measurement each minute of PMMR examination) were calculated for each corpse.

All measured quantitative T1, T2 and PD values were corrected for an arbitrary temperature of 37 °C for each single corpse. The method used for temperature correction was according to previous quantitative PMMR studies from Zech et al. [26,30], Schwendener et al. [28] and Persson et al. [29]. In this method, equations from plots of T1/temperature, T2/temperature and PD/temperature relationships of all investigated corpses are generated (see Table 1). Equations are used to correct values of T1, T2, and PD to a temperature of 37 °C by the following procedure: calculated core temperatures of each single corpse were subtracted from 37 °C (resulting temperatures are called Δ temperatures in the following). Δ temperatures were inserted in the equations generated from quantitative values/temperature plots (see Table 1) to gain ΔT1, ΔT2, and ΔPD values for each single corpse. Δ values were added to the uncorrected quantitative T1, T2, and PD values of each single corpse to gain temperature corrected values.

An example of temperature correction is shown for a grey matter T1 value In the following: The equation generated for grey matter T1/temperature plots was: y = 9.8 T + 885. An exemplary case had a temperature of 27 °C and a measured T1 grey matter value (not corrected for temperature) of 1163 ms. Δ temperature (37 °C minus 27 °C) was 10. Temperature corrected T1 value (ΔT1) based on equation was 9.8 × 10 = 98. ΔT1 value of 98 was added to 1163 ms resulting in a temperature corrected T1 value of 1261 ms.

2.6. Statistics

All statistical analyses were conducted using the SPSS® software package (Version 23.0). For each single corpse, the arithmetic mean of six single quantitative T1, T2 and PD measurements (not corrected for temperature) of each investigated anatomical brain structure were calculated. These values were used to calculate the arithmetic means and standard deviations of T1, T2 and PD values for all brain structures of all investigated (n = 50) corpses. The latter procedure was applied for temperature corrected T1, T2 and PD values also.

A series of one-way Welch F test ANOVAs with post hoc analysis was applied to evaluate differentiability of different brain structures based on their temperature corrected quantitative T1, T2, and PD values. Accuracy of discrimination between brain structures was described by the receiver operator characteristic (ROC) curve and the area under the ROC curve (AUC) with the traditional academic point system (0.90–0.1 = excellent, 0.80–0.90 = good, 0.70–0.80 = fair, 0.60–0.70 = poor, and 0.50–0.60 = fail) as described in previous quantitative PMMR studies [26,28–30].

Intra-observer error of quantitative brain T1 / T2 / PD measurements was estimated using a random selection of 20 cases of the study group. After a time lapse of one month, grey matter T1 / T2 / PD values were re-measured in the same quantitative PMMR dataset by the same observer (observer one). Two observers (observer one and observer two) independently measured T1 / T2 / PD values of the same PMMR datasets. For assessment of intra-observer error and inter-observer error the difference between two T1 / T2 / PD (not corrected for temperature) measurement series (observer one vs observer one; observer one vs observer two) were calculated. ANOVA testing was applied to evaluate the significance of the measuring differences.

3. Results

All investigated n = 50 brains showed signs of slight cerebral edema at histologic examinations. Other than that, histologic examinations did not show other relevant brain pathology. Cerebral edema was not visible in any of the conducted PMMR sequences.

Table 2
Mean quantification values (T1 and T2 in ms; PD in %) and standard deviations (SD) of the measured brain structures in cerebrum (Group 1) and brainstem/cerebellum (Group 2). Values are shown with and without temperature correction to 37 °C. Notice there is a decrease of standard deviations in temperature corrected T1 values.

	T1 uncorrected (SD)	T1 37 °C (SD)	T2 uncorrected (SD)	T2 37 °C (SD)	PD uncorrected (SD)	PD 37 °C (SD)
Group 1						
Grey matter	1113 (40)	1246 (23)	96 (12)	95 (1)	82 (9)	90 (8)
White matter	699 (37)	745 (19)	86 (13)	90 (10)	63 (11)	65 (9)
Thalamus	766 (46)	806 (31)	73 (8)	81 (7)	65 (4)	70 (3)
Caudate nucleus	908 (44)	975 (19)	65 (10)	75 (9)	67 (6)	71 (7)
Globus pallidus	777 (49)	815 (20)	62 (13)	69 (11)	60 (6)	68 (5)
Putamen	711 (31)	757 (21)	54 (7)	55 (7)	68 (5)	77 (4)
Internal capsule	888 (36)	915 (22)	91 (12)	91 (10)	56 (6)	61 (6)
Group 2						
Cerebral peduncle	960 (44)	1145 (22)	94 (14)	112 (13)	67 (6)	74 (5)
Substantia nigra	870 (31)	972 (19)	85 (12)	88 (11)	63 (7)	67 (6)
Red nucleus	858 (55)	903 (30)	89 (14)	98 (12)	56 (4)	57 (3)
Pons	726 (48)	803 (21)	85 (6)	82 (5)	60 (6)	61 (5)
Middle cerebellar peduncle	780 (54)	895 (31)	84 (12)	86 (12)	63 (4)	66 (4)
Cerebellar hemisphere	886 (43)	971 (25)	68 (7)	71 (5)	69 (3)	74 (2)
Medulla oblongata	987 (32)	1030 (18)	91 (9)	106 (8)	71 (3)	76 (3)

Table 3
Results of ANOVA testing of T1 (ms), T2 (ms), and PD (%) values (corrected to a temperature of 37 °C) in cerebrum (Group 1) and brainstem/cerebellum (Group 2). A significant difference between all tested brain structures was determined in each group. Accuracy of discrimination between anatomical structures was excellent or good in all tested pairs of both groups according to the area under the ROC curve.

	p value	Significance	ROC-AUC / accuracy
Group 1			
Grey matter-white matter	< 0.05	yes	0.96 / excellent
Grey matter-caudate nucleus	< 0.05	yes	1 / excellent
Grey matter-putamen	< 0.05	yes	1 / excellent
Grey matter-globus pallidus	< 0.05	yes	0.98 / excellent
Grey matter-thalamus	< 0.05	yes	1 / excellent
Grey matter-internal capsule	< 0.05	yes	0.92 / excellent
White matter-caudate nucleus	< 0.05	yes	0.90 / excellent
White matter-putamen	< 0.05	yes	0.95 excellent
White matter-globus pallidus	< 0.05	yes	0.88 / good
White matter-thalamus	< 0.05	yes	0.90 / excellent
White matter-internal capsule	< 0.05	yes	0.82 / good
Caudate nucleus-putamen	< 0.05	yes	0.88 / good
Caudate nucleus-globus pallidus	< 0.05	yes	0.84 / good
Caudate nucleus-thalamus	< 0.05	yes	0.80 / good
Caudate nucleus-internal capsule	< 0.05	yes	0.85 / good
Putamen-globus pallidus	< 0.05	yes	0.90 / excellent
Putamen-thalamus	< 0.05	yes	0.91 / excellent
Putamen-internal capsule	< 0.05	yes	0.98 / excellent
Globus pallidus-thalamus	< 0.05	yes	0.80 / good
Globus pallidus-internal capsule	< 0.05	yes	0.80 / good
Thalamus-internal capsule	< 0.05	yes	0.80 / good
Group 2			
Cerebral peduncle-substantia nigra	< 0.05	yes	1 / excellent
Cerebral peduncle-red nucleus	< 0.05	yes	1 / excellent
Cerebral peduncle-pons	< 0.05	yes	1 / excellent
Cerebral peduncle-middle cerebellar peduncle	< 0.05	yes	0.94 / excellent
Cerebral peduncle-cerebellum	< 0.05	yes	0.85 / good
Cerebral peduncle-medulla oblongata	< 0.05	yes	0.80 / good
Substantia nigra-red nucleus	< 0.05	yes	0.88 / good
Substantia nigra-pons	< 0.05	yes	0.80 / good
Substantia nigra-middle cerebellar peduncle	< 0.05	yes	0.81 / good
Substantia nigra-medulla oblongata	< 0.05	yes	0.95 / excellent
Substantia nigra-cerebellum	< 0.05	yes	0.90 / excellent
Red nucleus-pons	< 0.05	yes	0.84 / good
Red nucleus-middle cerebellar peduncle	< 0.05	yes	0.82 / good
Red nucleus-cerebellum	< 0.05	yes	1 / excellent
Red nucleus-medulla oblongata	< 0.05	yes	0.89 / good
Pons-middle cerebellar peduncle	< 0.05	yes	0.91 / excellent
Pons-cerebellum	< 0.05	yes	0.93 / excellent
Pons-medulla oblongata	< 0.05	yes	1 / excellent
Middle cerebellar peduncle-cerebellum	< 0.05	yes	0.88 / good
Middle cerebellar peduncle-medulla oblongata	< 0.05	yes	0.85 / good
Cerebellum-medulla oblongata	< 0.05	yes	0.83 / good

Table 1 gives the temperature-associated equations generated for Group 1 and Group 2 based on quantitative brain structure values / temperature plots. Mainly T1 values exhibited temperature dependence as they were increasing along with increasing core body temperatures. T2 values and PD values were influenced by temperature slightly only.

Table 2 shows the mean quantitative T1, T2 and PD values (corrected for temperature and not corrected for temperature) and standard deviations assessed for cerebrum in Group 1 and brainstem as well as cerebellum in Group 2. Temperature correction of quantitative values led to a general decrease of standard deviations in all investigated brain structures. In both groups, ANOVA testing showed significant differences of T1, T2 and PD values between different brain structures (Table 3) with at least good discrimination of brain structures based on the Area under the ROC curve (Table 4). Fig. 2 shows tight clustering of individual brain structure values in both groups.

Table 4
Results for intra- and inter-observer error estimation of T1, T2 and PD measurements. ANOVA testing showed no significant differences for measurements of the same observer or two different observers, indicating non-relevant intra-observer or inter-observer variability.

	Mean difference T1 / T2 / PD	Min – max difference T1 / T2 / PD	p - value
Intra-observer	17 / 3 / 6	3–21 / 0–7 / 0.5–8	0.081
Inter-observer	15 / 4 / 7	4–19 / 0–8 / 0–9	0.076

Inter- and intra-observer error analysis indicated non-significant inter- or intra-observer variability of measured quantitative brain values (Table 4).

4. Discussion

The results of the present 3 Tesla PMMR study indicate, that regular anatomical structure of cerebrum, cerebellum and brainstem may be characterized and discerned based on their quantitative T1, T2 and PD values. The study results are in accordance with previous PMMR studies that demonstrated discernibility of anatomical brain structures for 1.5 Tesla applications [30,35]. In living patients, T1 brain values increase as magnetic field strength increases. In a range of 0.3–3 Tesla, T1 values may double due to decrease of fraction of protons able to interact at higher Larmor frequency. At the same time, T2 values may decrease due to mechanisms of T2 relaxation such as chemical exchange and molecular diffusion [36–39]. When comparing the evaluated 3 T PMMR values of the present study with known 1.5 T PMMR values, similar observations occur for the post-mortem brain: 3 T PMMR T1 values of the same anatomical brain structures were clearly higher than 1.5 PMMR T1 values while 3 T PMMR T2 values decreased. For instance, white matter in a previous PMMR 1.5 T study exhibited temperature corrected (37 °C) mean T1 values of 478 ms and T2 values of 130 ms. In the present 3 T PMMMR study temperature corrected (37 °C) mean T1 values were 745 ms and T2 values 90 ms respectively. Proton density was almost identical for both studies with 67% in 1.5 T and 65% in 3 T [30]. These observations showed, that 3 T and 1.5 T T1 and T2 PMMR brain values need to be treated separately when being used for post-mortem diagnostics. Moreover, temperature dependence needs to be considered, in particular for T1 values. In accordance with previous PMMR studies, T1 values in the present study showed a rather linear increase with rising corpse temperatures while T2 and PD values were only slightly influenced [26,33,34]. These findings demonstrate the need for temperature correction of quantitative values when being used for further diagnostics. The equations generated in the present study may be used for temperature correction of 3 T PMMR quantitative values.

Future 3 T PMMR studies need to evaluate the quantitative values of pathologic or traumatic brain lesions such as hemorrhage, infarction, and tumors. Previous quantitative PMMR studies already demonstrated the potential of synthetic PMMR for characterization and differentiation of soft tissue and organ lesions [27–29]. If quantitative PMMR values of regular anatomical brain structures, lesions, and pathologies are known, they may be used for advanced diagnostics in post-mortem neuroimaging. The methods allows forensic radiologists performing measurements in visible brain signal alterations. Based on knowledge of regular and pathologic quantitative values, such measurements may provide additional information on brain pathology and traumatic lesions. Such

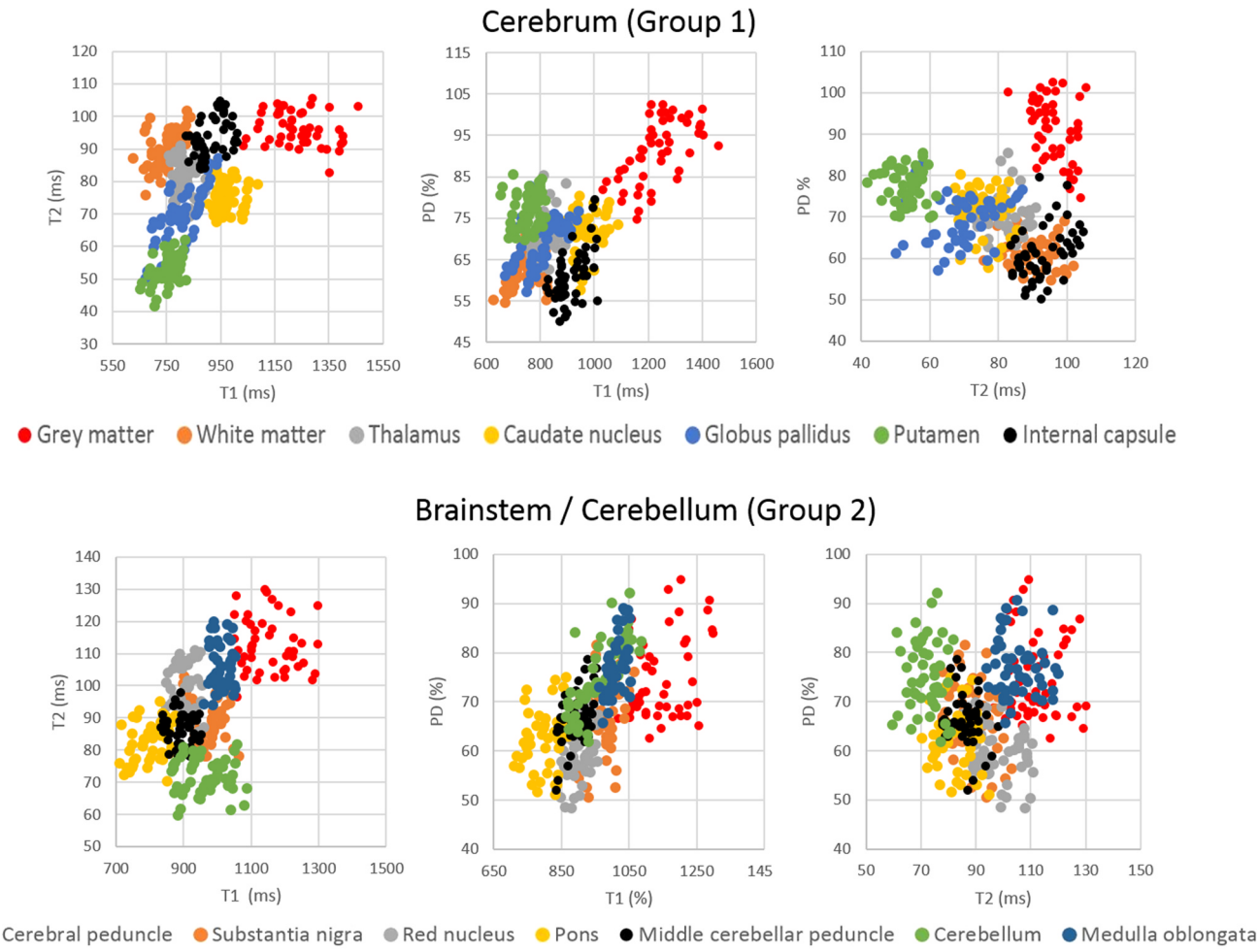

Fig. 2. Plots of quantitative values (corrected for a temperature of 37 °C) of assessed anatomical structures of cerebrum (Group 1) and brainstem/cerebellum (Group 2). Three views (T2/T1, PD/T1, and PD/T2 view) are shown for each group. In both groups, best visual differentiation of clusters can be observed in T2/T1 views.

information may for example be a more specific age estimation of hemorrhage or infarction. However, without further studies on brain pathology it can only be speculated how useful such measurements would be. The quantitative approach may also enable post-mortem computer-aided detection and diagnosis (CAD) [40,41]. In synthetic PMMR datasets, each voxel contains information on T1, T2 and PD [25]. This provides a base for segmentation of datasets with dedicated software able to detect relevant lesions and pathology in the brain. In theory, this is not only possible for the brain but the whole human body. Such software could be implemented in radiological workstations to aid forensic pathologists and forensic radiologists in routine forensic casework.

Future quantitative PMMR studies may also extend to 7 Tesla applications since different T1 and T2 relaxation times are expected compared to 1.5 T and 3 T applications. So far, only few 7 T PMMR studies were conducted on solitary brain specimens [42]. However, increasing use of 7 T applications in post-mortem imaging can be expected in the future.

Limitations: Quantitative brain values were obtained from n = 50 cases only. If quantitative PMMR is to be used for future advanced diagnostics, a reference brain T1, T2, and PD database based on more cases is required both for 1.5 T and 3 T applications. It can be expected that larger datasets result in smaller standard errors (standard deviations respectively). Smaller standard deviations would mean less overlapping between the values of different anatomical structures and therefore possibly improve differentiability.

All investigated brains showed histological signs of slight cerebral edema which is a common post-mortem finding. So far it is unknown, if slight brain edema causes significant changes of quantitative T1, T2 and PD values compared to post-mortem brains showing either no signs of edema or severe signs of edema. This study only relies on regular findings (with the exception of edema). Thus, it remains unclear how pathologic tissue variations would specifically alter quantitative values.

5. Conclusion

Temperature corrected PMMR 3 Tesla T1, T2, and PD values are feasible for discrimination of regular anatomical brain structures of cerebrum, brainstem, and cerebellum. The quantitative approach provides a base for future computer-aided detection of forensically relevant brain findings in PMMR.

Funding

This study received no funding.

CRediT authorship contribution statement

Isabel Arnold: Methodology, Formal analysis, Investigation, Writing – original draft, Visualization. **Nicole Schwendener:** Formal analysis, Data Curation, Writing – review & editing. **Paolo**

Lombardo: Writing – review & editing. **Christian Jackowski:** Conceptualization, Methodology, Resources, Writing – review & editing. **Wolf-Dieter Zech:** Conceptualization, Methodology, Validation, Formal analysis, Writing – review & editing, Visualization, Supervision, Project administration.

Conflict of Interest

The authors declare that they have no conflict of interest.

Acknowledgements

We would like to express our gratitude to our team of forensic pathologists and forensic technicians for their support with case handling.

Compliance with ethical standards

This manuscript does not contain any studies with live human participants or animals.

Usage of the acquired data was approved by the local ethics committee.

References

[1] T.D. Ruder, M.J. Thali, G.M. Hatch, Essentials of forensic post-mortem MR imaging in adults, Br. J. Radiol. 87 (1036) (2014) 20130567.
[2] C. Jackowski, A. Christe, M. Sonnenschein, E. Aghayev, M.J. Thali, Postmortem unenhanced magnetic resonance imaging of myocardial infarction in correlation to histological infarction age characterization, Eur. Heart J. 27 (20) (2006) 2459–2467 Epub 2006 Sep 14.
[3] L. Patriquin, A. Kassarjian, M. Barish, L. Casserley, M. O'Brien, C. Andry, S. Eustace, Postmortem whole-body magnetic resonance imaging as an adjunct to autopsy: preliminary clinical experience, J. Magn. Reson Imaging 13 (2) (2001) 277–287.
[4] I.S. Roberts, E.W. Benbow, R. Bisset, J.P. Jenkins, S.H. Lee, H. Reid, A. Jackson, Accuracy of magnetic resonance imaging in determining cause of sudden death in adults: comparison with conventional autopsy, Histopathology 42 (5) (2003) 424–430.
[5] R. Dirnhofer, C. Jackowski, P. Vock, K. Potter, M.J. Thali, VIRTOPSY: minimally invasive, imaging-guided virtual autopsy, Radiographics 26 (5) (2006) 1305–1333 1305-1033.
[6] S. Addison, O.J. Arthurs, S. Thayyil, Post-mortem MRI as an alternative to non-forensic autopsy in foetuses and children: from research into clinical practice, Br. J. Radiol. 87 (1036) (2014) 20130621, https://doi.org/10.1259/bjr.20130621
[7] C. Jackowski, N. Schwendener, S. Grabherr, A. Persson, Post-mortem cardiac 3-T magnetic resonance imaging: visualization of sudden cardiac death? J. Am. Coll. Cardiol. 62 (7) (2013) 617–629, https://doi.org/10.1016/j.jacc.2013.01.089 Epub 2013 Apr 3.
[8] C. O'Donnell, N. Woodford, Post-mortem radiology–a new sub-speciality? Clin. Radiol. 63 (11) (2008) 1189–1194, https://doi.org/10.1016/j.crad.2008.05.008 Epub 2008 Sep 3.
[9] S. Grabherr, C. Egger, R. Vilarino, L. Campana, M. Jotterand, F. Dedouit, Modern post-mortem imaging: an update on recent developments, Forensic Sci. Res. 2 (2) (2017) 52–64, https://doi.org/10.1080/20961790.2017.1330738 eCollection 2017.
[10] P.M. Flach, M.J. Thali, T. Germerott, Times have changed! Forensic radiology–a new challenge for radiology and forensic pathology, AJR Am. J. Roentgenol. 202 (4) (2014) W325–W334, https://doi.org/10.2214/AJR.12.10283
[11] G. Ampanozi, D. Halbheer, L.C. Ebert, M.J. Thali, U. Held, Postmortem imaging findings and cause of death determination compared with autopsy: a systematic review of diagnostic test accuracy and meta-analysis, Int. J. Leg. Med. 134 (1) (2020) 321–337, https://doi.org/10.1007/s00414-019-02140-y Epub 2019 Aug 27.
[12] C. Lundström, A. Persson, S. Ross, et al., State-of-the-Art of Visualization in Post-Mortem Imaging, APMIS, 2012, pp. 316–326 120 (4).
[13] S. Grabherr, J. Grimm, P. Baumann, P. Mangin, Application of contrast media in post-mortem imaging (CT and MRI), Radiol. Med. 120 (9) (2015) 824–834, https://doi.org/10.1007/s11547-015-0532-2 Epub 2015 Apr 5. Review.
[14] J. Tschui, C. Jackowski, N. Schwendener, C. Schyma, W.D. Zech, Post-mortem CT and MR brain imaging of putrefied corpses, Int. J. Leg. Med. 130 (4) (2016) 1061–1068.
[15] T.M. Schmidt, R. Fischer, S. Acar, M. Lorenzen, A. Heinemann, U. Wedegärtner, G. Adam, J. Yamamura, DWI of the brain: postmortal DWI of the brain in comparison with in vivo data, Forensic Sci. Int. 220 (1–3) (2012) 180–183.
[16] K. Yen, K.O. Lövblad, E. Scheurer, C. Ozdoba, M.J. Thali, E. Aghayev, C. Jackowski, J. Anon, N. Frickey, K. Zwygart, J. Weis, R. Dirnhofer, Post-mortem forensic neuroimaging: correlation of MSCT and MRI findings with autopsy results, Forensic Sci. Int 173 (1) (2007) 21–35.
[17] P.M. Flach, S. Schroth, W. Schweitzer, G. Ampanozi, J. Slotboom, C. Kiefer, T. Germerott, M.J. Thali, M. El-Koussy, Deep into the fibers! postmortem diffusion tensor imaging in forensic radiology, Am. J. Forensic Med. Pathol. 36 (2015) 153–161.
[18] O.J. Arthurs, G.C. Price, D.W. Carmichael, R. Jones, W. Norman, A.M. Taylor, N.J. Sebire, Diffusion-weighted perinatal postmortem magnetic resonance imaging as a marker of postmortem interval, Eur. Radio. 25 (5) (2015) 1399–1406.
[19] E. Scheurer, K.O. Lovblad, R. Kreis, S.E. Maier, C. Boesch, R. Dirnhofer, K. Yen, Forensic application of postmortem diffusion-weighted and diffusion tensor MR imaging of the human brain in situ, AJNR Am. J. Neuroradiol. 32 (8) (2011) 1518–1524.
[20] E. Aghayev, K. Yen, M. Sonnenschein, C. Ozdoba, M. Thali, C. Jackowski, R. Dirnhofer, Virtopsy post-mortem multi-slice computed tomography (MSCT) and magnetic resonance imaging (MRI) demonstrating descending tonsillar herniation: comparison to clinical studies, Neuroradiology 46 (7) (2004) 559–564.
[21] J.B. Warntjes, O. Dahlqvist, P. Lundberg, Novel method for rapid, simultaneous T1, T*2, and proton density quantification, Magn. Reson. Med. 57 (2007) 528–537.
[22] J.B. Warntjes, O.D. Leinhard, J. West, P. Lundberg, Rapid magnetic resonance quantification on the brain: optimization for clinical usage, Magn. Reson. Med. 60 (2008) 320–329.
[23] M.J. Warntjes, J. Kihlberg, J. Engvall, Rapid T1 quantification based on 3D phase sensitive inversion recovery, BMC Med. Imaging 10 (2010) 19.
[24] I. Blystad, J.B. Warntjes, O. Smedby, A.M. Landtblom, P. Lundberg, E.M. Larsson, Synthetic MRI of the brain in a clinical setting, Acta Radiol. 53 (2012) 1158–1163.
[25] C. Jackowski, M.J. Warntjes, J. Kihlberg, J. Berge, M.J. Thali, A. Persson, Quantitative MRI in isotropic spatial resolution for forensic soft tissue documentation.Why and how? J. Forensic Sci. 56 (1) (2011) 208–215.
[26] W.D. Zech, N. Schwendener, A. Persson, M.J. Warntjes, C. Jackowski, Temperature dependence of postmortem MR quantification for soft tissue discrimination, Eur. Radiol. 25 (8) (2015) 2381–2389.
[27] W.D. Zech, N. Schwendener, A. Persson, M.J. Warntjes, C. Jackowski, M.R. Postmortem, quantification of the heart for characterization and differentiation of ischaemic myocardial lesions, Eur. Radiol. 25 (7) (2015) 2067–2073.
[28] N. Schwendener, C. Jackowski, A. Persson, M.J. Warntjes, F. Schuster, F. Riva, W.D. Zech, Detection and differentiation of early acute and following age stages of myocardial infarction with quantitative post-mortem cardiac 1.5T MR, Forensic Sci. Int. 270 (2017) 248–254, https://doi.org/10.1016/j.forsciint.2016.10.014 Epub 2016 Oct 24.
[29] A. Persson, J. Baeckmann, J. Berge, C. Jackowski, M. Warntjes, W.D. Zech, Temperature-corrected postmortem 3-T MR quantification of histopathological early acute and chronic myocardial infarction: a feasibility study, Int. J. Leg. Med. 132 (2) (2018) 541–549, https://doi.org/10.1007/s00414-017-1614-6 Epub 2017 Jun 13..
[30] W.D. Zech, A.L. Hottinger, N. Schwendener, F. Schuster, A. Persson, M.J. Warntjes, C. Jackowski, Post-mortem 1.5T MR quantification of regular anatomical brain structures, Int. J. Leg. Med. 130 (4) (2016) 1071–1080.
[31] M.E. Haacke, R.W. Brown, M.R. Thompson, N. Venkatesh, Magnetization, relaxation and the bloch equation, Magnetic Resonance Imaging-Physical Principles and Sequence Design, first ed., John Wiley & Sons, New York, NY, 1999, pp. 51–62.
[32] K. Tashiro, S. Shiotani, T. Kobayashi, K. Kaga, H. Saito, S. Someya, K. Miyamoto, H. Hayakawa, Cerebral relaxation times from postmortem MR imaging of adults, Magn. Reson. Med. Sci. 14 (1) (2015) 51–56.
[33] T.D. Ruder, G.M. Hatch, L. Siegenthaler, G. Ampanozi, S. Mathier, M.J. Thali, O.M. Weber, The influence of body temperature on image contrast in post mortem MRI, Eur. J. Radiol. 81 (2012) 1366–1370.
[34] C. Birkl, C. Langkammer, J. Haybaeck, C. Ernst, R. Stollberger, F. Fazekas, S. Ropele, Temperature-induced changes of magnetic resonance relaxation times in the human brain: a postmortem study. Magn. Reson. Med. 71 (4) (2014) 1575–1580.
[35] P.A. Bottomley, T.H. Foster, R.E. Argersinger, L.M. Pfeifer, A review of normal tissue hydrogen relaxation times and relaxation mechanisms from 1–100 MHz: dependence on tissue type, NMR frequency, temperature, species, excision, and age, Med. Phys. 11 (1984) 425–448.
[36] R.A. De Graaf, P.B. Brown, S. McIntyre, T.W. Nixon, K.L. Behar, D.L. Rothman, High magnetic field water and metabolite proton T1 and T2 relaxation in rat brain in vivo, Magn. Reson. Med. 56 (2006) 386–394.
[37] J.-P. Korb, R.G. Bryant, Magnetic field dependence of proton spin-lattice relaxation times, Mag. Reson. Med. 48 (2002) 21–26.
[38] W.D. Rooney, G. Johnson, X. Li, E.R. Cohen, S.G. Kim, K. Ugurbil, Jr Springer CS, Magnetic field and tissue dependencies of human brain longitudinal 1H20 relaxation in vivo, Mag. Reson. Med. 57 (2007) 308–318.
[39] G.J. Stanisz, E.E. Odrobina, J. Pun, M. Escaravage, S.J. Graham, M.J. Bronskill, R.M. Henkelman, T1, T2 relaxation and magnetization transfer in tissue at 3T, Magn. Reson. Med. 54 (2005) 507–512.
[40] V. Giannini, S. Mazzetti, A. Vignati, F. Russo, E. Bollito, F. Porpiglia, M. Stasi, D. Regge, A fully automatic computer aided diagnosis system for peripheral zone prostate cancer detection using multi-parametric magnetic resonance imaging, Comput. Med. Imaging Graph. 46 (Pt 2) (2015) 219–226.
[41] Y. Wu, R. Yang, S. Jia, Z. Li, Z. Zhou, T. Lou, Computer-aided diagnosis of early knee osteoarthritis based on MRI T2 mapping, Biomed. Mater. Eng. 24 (6) (2014) 3379–3388.
[42] H. Lee, S.Y. Baek, S.Y. Chun, J.H. Lee, H. Cho, Specific visualization of neuromelanin-iron complex and ferric iron in the human post-mortem substantia nigra using MR relaxometry at 7T, Neuroimage 172 (2018) 874–885.